Planetary and Space Science 75 (2013) 158–166

Contents lists available at SciVerse ScienceDirect

Planetary and Space Science

journal homepage: www.elsevier.com/locate/pss

Short Communication

Investigation and remediation of false topographic perception phenomena observed on Chang'E-1 lunar imagery

Bo Wu [a,*], Haifeng Li [a,b], Yang Gao [a]

[a] Department of Land Surveying & Geo-Informatics, The Hong Kong Polytechnic University, Hung Hom, Kowloon, Hong Kong
[b] School of Geosciences and Info-Physics, Central South University, Changsha, China

ARTICLE INFO

Article history:
Received 31 July 2012
Received in revised form
18 October 2012
Accepted 31 October 2012
Available online 8 November 2012

Keywords:
Lunar topography
Chang'E-1
FTPP
Wavelet transform

ABSTRACT

False topographic perception phenomenon (FTPP) is a relief inversion phenomenon in remote sensing images and causes false perception problems. Such images of the Moon suffer from serious FTPP problems. Correctly observing and understanding the terrain features on the Moon from lunar surface images is important for lunar exploration missions and various lunar scientific investigations. This paper presents a systematic investigation of the FTPP problem associated with lunar craters, by using the Chang'E-1 lunar imagery covering the major areas of the lunar surface. Results reveal that the FTPP problem is positively correlated with crater latitudes in the north hemisphere of the Moon. For craters within a similar latitude range, the FTPP level is positively correlated with the depth–diameter ratio of the crater. A wavelet-transform based approach is proposed for FTPP remediation on Chang'E-1 imagery. Experimental analysis using three different types of craters revealed that the approach is able to effectively correct the FTPP problem.

1. Introduction

False topographic perception phenomenon (FTPP) is a relief inversion problem firstly identified by Saraf et al. (1996) in Earth remote sensing images. FTPP is commonly observed in Earth images of rugged terrain surfaces acquired from Sun-synchronous satellites (e.g., Landsat, IKONOS), and it causes topographic perception problems, i.e., mountains appear as valleys, craters appear as hillocks, and vice versa (Saraf et al., 1996; Rudnicki, 2000; Patterson and Kelso, 2004). The FTPP problem has also been noticed on lunar images (Saraf et al., 2011). Remote sensing images of the Moon surface, in fact, suffer from more serious FTPP problems. This is mainly due to the highly rugged and dust grayout surface, the absence of atmosphere eliminates the scattering effects, and the lack of familiar landmarks on the Moon, to supply visual cues (Colby, 1991; Rieser et al., 1995).

Fig. 1 illustrates typical examples of lunar images suffering from FTPP problems. Fig. 1(a) shows a crater in the Chinese Chang'E-1 image recognized as a hillock as a result of the FTPP problem. After the image is rotated by 180°, it appears as a crater free of FTPP as shown in Fig. 1(b). Fig. 1(c) and (d) illustrate a similar example on the India Chandrayaan-1 image. Fig. 1(e) and (f) show other similar examples as observed in NASA's Lunar Reconnaissance Orbiter (LRO) Narrow Angle Camera (NAC) image. These images were taken by different sensors at different time slots, and have different spatial resolutions, such as 120 m/pixel for the Chang'E-1 imagery (Ouyang et al., 2010), 5 m/pixel for the Chandrayaan-1 imagery (Kumar and Chowdhury, 2005), and 0.5 m/pixel for the LRO NAC imagery (Robinson et al., 2010). This indicates that the FTPP problem is quite common in lunar surface images from different sources with different resolutions.

Many factors lead to the FTPP problem such as topographic relief, object locations, Sun elevation and azimuth angles, viewing angle, and hatching or engraving features presented on the valley slopes (Saraf et al., 2005). Liu and Todd (2004) and Saraf et al. (2005, 2007) provide several solutions for FTPP remediation on Earth surface images. However, this problem has not been investigated systematically, in particular for lunar surface imagery.

The lunar terrain is highly irregular and rugged. There are about half a million craters on the Moon with diameters greater than 1 km (Ivanov, 2001). Correctly observing and understanding the terrain features from lunar surface images is important. Lunar images with FTPP problems inhibit accurate scientific study of the Moon. During the planning of lunar robotic or human exploration missions, any wrong interpretation of the lunar surface because of FTPP must be avoided. Systematic investigation of the FTPP problem in lunar surface imagery and the remediation methods for the FTPP problem are vital to support future lunar exploration missions and various lunar scientific investigations.

This paper presents a systematic investigation of the FTPP problems observed in the Chang'E-1 imagery and an effective

* Corresponding author. Tel.: +852 2766 4335; fax: +852 2330 2994.
E-mail address: bo.wu@polyu.edu.hk (B. Wu).

0032-0633/$ - see front matter © 2012 Elsevier Ltd. All rights reserved.
http://dx.doi.org/10.1016/j.pss.2012.10.018

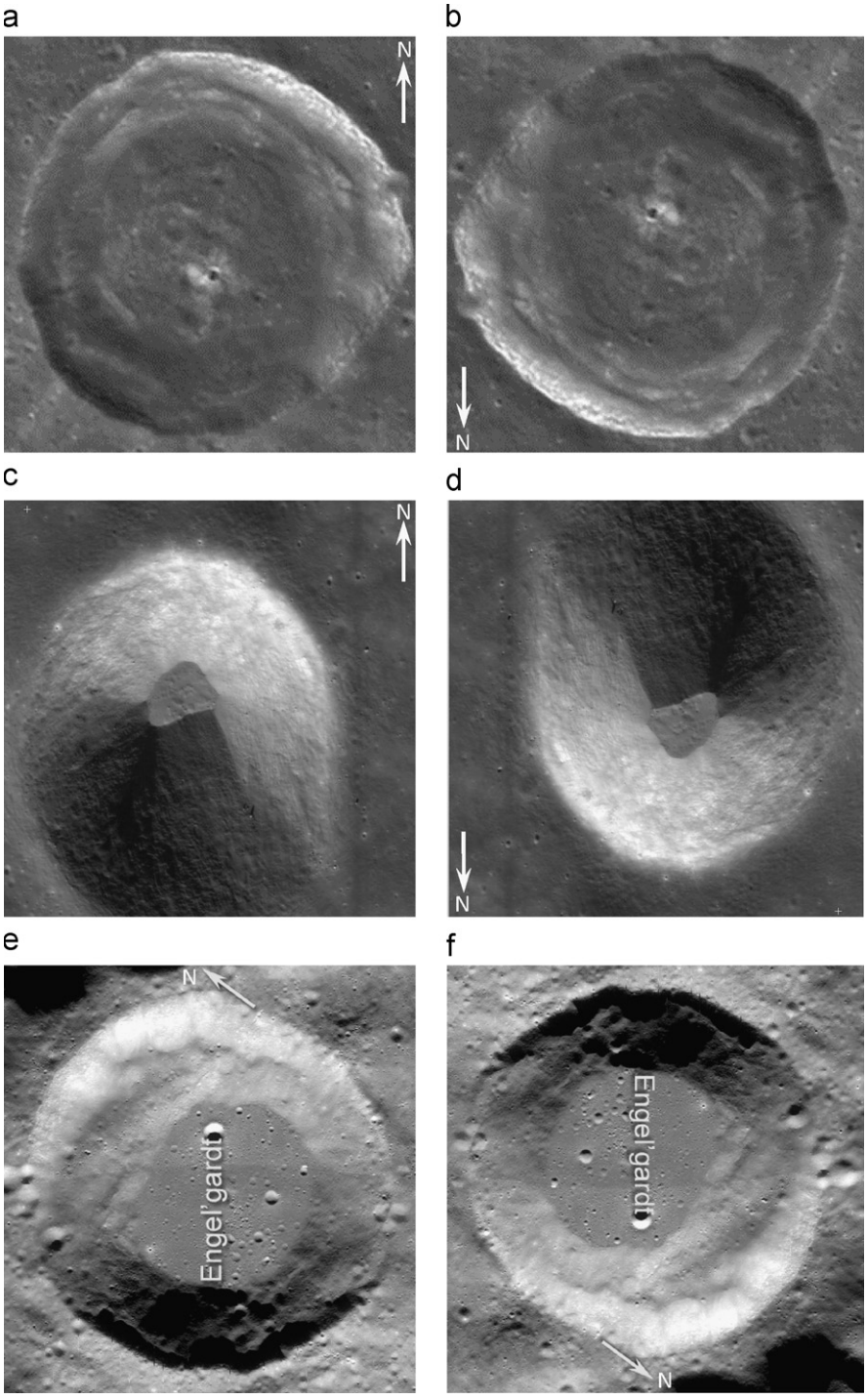

Fig. 1. Examples of FTPP observed on lunar orbit imagery: (a) An original Chang'E-1 image with FTPP, (b) the Chang'E-1 image rotated by 180° free of FTPP, (c) an original Chandrayaan-1 image with FTPP, (d) the Chandrayaan-1 image rotated by 180° free of FTPP, (e) an original LRO image with FTPP, and (f) the LRO image rotated by 180° free of FTPP.

method alleviating the FTPP problems. The paper is organized as follows. A literature review of existing studies of FTPP problems and FTPP correction methods is given in the second section. A systematic statistical analysis of the FTPP problem discovered in Chang'E-1 imagery is presented in the third section. A wavelet-transform based approach for FTPP remediation is presented in the fourth section and the detailed experimental results and analysis are also given in the fourth section. Finally, conclusions are presented and discussed.

2. Related work

It is generally recognized that vision perception plays a major role in remote sensing image cognition (Toutin, 1998). The FTPP problem in remote sensing imagery is mainly due to human perception. Human brain perceives that light illuminating source is from northern hemisphere (front) rather than from southern hemisphere (behind). Human vision relies heavily on lighting cues to recover 3D shape (Morgenstern et al., 2011).

When estimating 3D shapes from shading, the human visual system resolves this ambiguity by relying on the prior knowledge of illumination from light-from-front.

Ramachandran (1988a) tested a series of shaded shapes and found human brains seem to accept that only one light source illuminates the whole image. The visual system also tends to assume the light comes from one natural source, namely from front. Ramachandran (1988a) pointed out the ambiguity of shaded shapes being perceived either pop-out or inward in certain circumstances because the brain does not know where the light will come from, causing the observer to mentally shift the light source to invert the object depth. Ramachandran (1988b) also suggested that certain features of objects, such as the raised rim of a crater leading to shadows with obvious directions, could inform the brain about the illumination direction. Thus the indication is that FTPP could be influenced by certain features of objects.

Attention has been drawn to FTPP by geographers because of problems indicated in the perception of remote sensing images. Patterson and Kelso (2004) noticed this false topographic perception phenomenon and named it "Relief Inverse". They also suggested some simple solutions such as using clone stamp tools to replace the shadows with neutral colours and textures. This technique, however, brings false texture information to the image and the result is poor. Saraf et al. (1996, 2005, and 2007) analysed the main factors leading to the FTPP problem in remote sensing images. They found that the north-west position is always adopted by human brains as the assumption of the sun-illumination position when perceiving the remote sensing images. If the actual sun-illumination position deviates from the assumption when collecting the remote sensing images, FTPP problems will occur, the intensity of which will depends on the degree of deviation. Several methods have been proposed to correct the FTPP problem in remote sensing images, such as image rotation (Saraf et al., 1996), inversion of digital number (DN) value (Saraf et al., 1996), shaded relief model (SRM) and hue-intensity-saturation (HIS) transformation (Saraf et al., 2005, 2007). The core idea for all these methods is to change the illumination direction of the remote sensing image to the north or front.

Image rotation refers to the rotation of the image by 180° (Saraf et al., 1996). It is the easiest way to remove the FTPP impact on remote sensing imagery as indicated by the examples in Fig. 1. However, image rotation will (1) make the north direction invert from the common, and (2) sometimes make the rotated image resemble a completely new one, bringing new problems in image perception. The DN value inversion method subtracts the grey value of each pixel by 255 (Saraf et al., 1996). This method can avoid inverted cartography, but the inversion will change other information on the image and lead to loss of original textural information.

Saraf et al. (2005) proposed a method by firstly transferring the image from the RGB format to the HIS format, then using the SRM to replace the intensity, and finally retransfer the image from HIS to RGB format. By incorporating the SRM, satisfactory results can be obtained without changing the map direction or natural object reflectance recorded in pixels. Saraf et al. (2007) suggested an efficient method to correct the FTPP problem. This method first transfers the RGB image into HIS format, then directly inverts the intensity channel, and finally transfers the image back from HIS to RGB format. This method however cannot process remote sensing images in black and white. Additionally, when inverting pixel intensity, the brightness of the image can overflow. This problem requires additional techniques to better balance the brightness of the intensity images.

Previous FTPP studies are mainly focused on Earth images. FTPP problems in lunar images have been seldom investigated, except the very recent work of Saraf et al. (2011), which demonstrated examples of serious FTPP problems as observed from the Chandrayan-1 images. However, Saraf et al. (2011) did not provide any new solution to resolve FTPP problems in lunar images.

Unlike previous work, this study focuses on the following two aspects: (1) A systematic study of the FTPP problem based on the Chang'E-1 imagery covering the major areas of the lunar surface. This has not been tackled before. (2) An effective approach for FTPP remediation of lunar imagery based on wavelet transform techniques.

3. Investigation of FTPP observed on Chang'E-1 imagery

The Chinese Chang'E-1 lunar probe was launched on October 24, 2007. The CCD camera on-board the Chang'E-1 successfully returned 1098 orbiter images, covering the whole lunar surface. A laser altimeter which generates range measurements covering the whole Moon, is on-board the Chang'E-1. The Chang'E-1 data set used in this study is the Level 2C data released by the Chinese Academy of Sciences, which has already been processed for radiometric, geometric, and spectrophotometric correction (CAS (Chinese Academy of Sciences), 2008; Ouyang et al., 2010). Since there are enormous numbers of craters on the Moon, this study focuses mainly on the FTPP problem associated with lunar craters. Other lunar terrain features, such as valleys and mountains in lunar images may also suffer from FTPP problems. The investigations and methods presented in this paper are also useful in better understanding and the subsequent solving of FTPP problems related to other lunar terrain features.

3.1. Observations of FTPP problem on Chang'E-1 imagery

Fig. 2 shows a mosaic of 313 tracks of Chang'E-1 imagery coverings the whole lunar surface. To systematically investigate the FTPP problem on Chang'E-1 imagery, 26 tracks of Chang'E-1 images were selected from the 313 tracks and evenly distributed on the lunar surface. It should be noted that this study aims to produce a representative study of the FTPP problem on the lunar surface. The selected study areas cover the latitudes from -70° to 70°. The extreme cases in the pole regions are not included in this study. Fig. 2 illustrates the coverage of the 26 selected tracks of images.

For each image track, two individual operators, trained to be familiar with the FTPP problem, examined the entire image and marked the craters which displayed obvious FTPP problems. Craters marked by both operators were identified as having FTPP problems in common. They are marked by white dots on Fig. 3. It should be noted that, only those craters which are clearly recognizable (with a diameter larger than 5 km) on Chang'E-1 imagery are considered in this interpretation process.

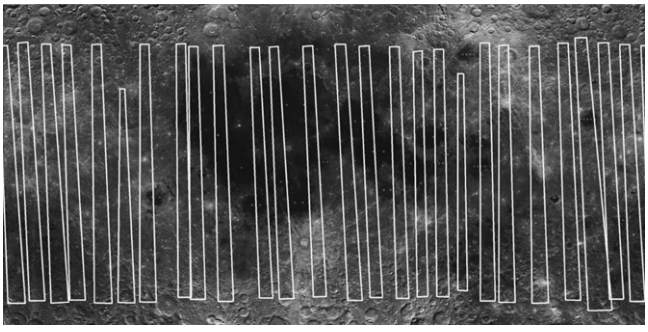

Fig. 2. A mosaic of the Chang'E-1 imagery covering the whole lunar surface and the distribution of the selected 26 tracks.

In Fig. 3, a total of 210 craters were identified as having FTPP problems. The crater locations (latitude and longitude of the centre), diameters, and depths were then determined based on the crater topographic models. The crater topographic models were generated by using the Chang'E-1 stereo imagery and Chang'E-1 laser altimeter through an integrated photogrammetric method (Wu et al., 2011). The resolution for the crater topographic models is 360 m. Detailed information of the identified craters is given in Table 1.

3.2. Analysis of factors related to FTPP problems

3.2.1. Relationship between FTPP and crater locations

To analyse the distribution of the craters with obvious FTPP problems, two histograms were generated with respect to the latitude and longitude of craters. They are shown, respectively, in Fig. 4(a) and (b).

From Fig. 4(a), it is clearly seen that the FTPP problem in the north hemisphere is more serious than that of the south, especially in the circumpolar regions. The FTPP trend is almost increasing progressive from the equator to the poles in the northern hemisphere. Illumination directions can be used to explain the significant unbalanced distribution of craters with FTPP between the two hemispheres as indicated in Fig. 3. The Moon and Earth have similar sun illumination conditions. Of these conditions the perpendicular incidence of sun illumination for the Moon is 1.6° while the perpendicular incidence is 23.5° for the Earth. Therefore, the part of the Moon beyond 1.6° latitude in the northern hemisphere will always have sun illumination from the south, while the part beyond −1.6° latitude in the southern hemisphere will always have sun illumination from the north. Referring to the assumption of light-from-front in human visual perception as discussed previously, the northern hemisphere will suffer more FTPP problems compared with the number suffered by the southern hemisphere. It can be concluded that the FTPP is positively correlated to the latitude in the northern hemisphere. The relationships can be generally modelled by a third-order polynomial as illustrated in Fig. 4(a). From the observation in this study, the north pole region suffers from extremely serious FTPP problems, a feature also been reported by Saraf et al. (2011).

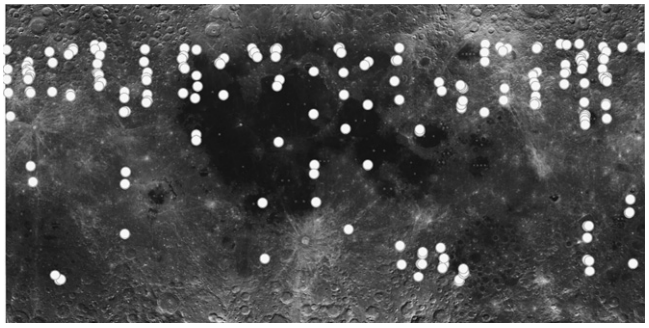

Fig. 3. Distributions of the craters suffering from obvious FTPP problems in the Chang'E-1 imagery.

Table 1
Summary of the craters with FTPP problems observed on Chang'E-1 imagery.

Total crater numbers	210	
Crater diameter	Maximum	80 km
	Minimum	5 km
	Mean	15.76 km
Crater depth	Maximum	6 km
	Minimum	0.4 km
	Mean	2.18 km

As for the craters identified with FTPP in the southern hemisphere, this could be explained by the following two reasons. First, the specific characteristics of some craters and the related illumination conditions on the images may affect the perception of the operator. For example, some crater may be perceived as hillock due to the relatively large protrusions inside the crater, and some large shallow crater might be perceived as pop-out when there is no much difference between the illumination condition of the crater and its nearby region. Second, the psychological process of the operator may influence the perception. When the operators examining each strip of the Chang'E-1 images from bottom (south) to top (north), it is more likely for them to identify craters with FTPP since they are undergoing a psychological process from light to heave FTPP situations and the comparison of craters in local regions may lead to deviated perceptions.

The craters with FTPP problems along the longitude direction are more evenly distributed as shown in Fig. 4(b). Therefore, it can be concluded that the FTPP is not related to the longitude.

3.2.2. Relationship between FTPP and crater shapes

Crater shape is another important factor related to FTPP. The ratio I (d/D) of rim-to-floor depth (d) to the rim-to-rim diameter (D) has been widely used in the past to characterize the crater shapes on the Moon and Mars (Moutsoulas and Preka, 1981; Stepinski, 2010). The smaller the I, the flatter the crater. This study also employs the ratio I of crater in the analysis of the relationship between FTPP and crater shapes.

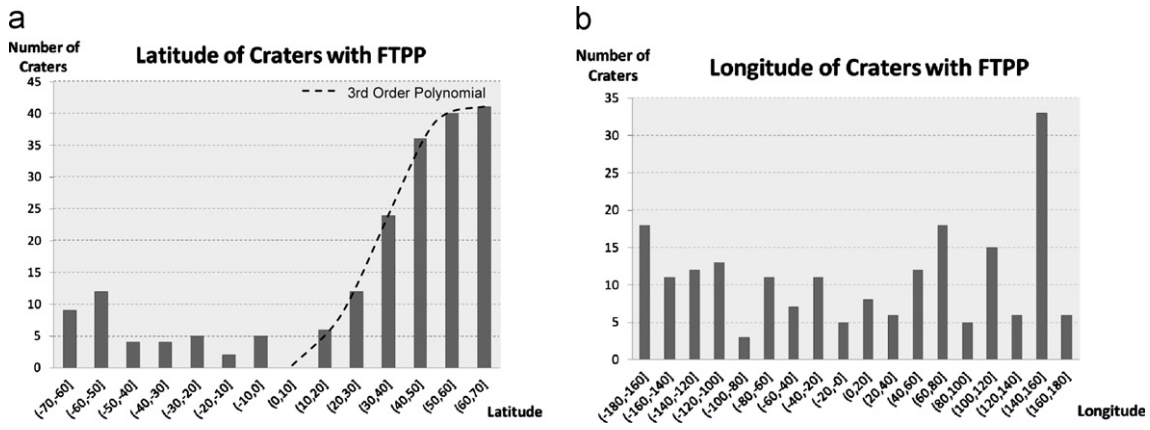

Fig. 4. Histograms of craters suffering from FTPP with respect to crater locations: (a) Number of craters with FTPP with respect to the crater latitudes, and (b) number of craters with FTPP with respect to the crater longitudes.

The FTPP situations of the craters are classified into five different levels (5–9) based on the serious of FTPP degrees, with 5 representing light FTPP and 9 representing heavy FTPP. Two individual operators examined all the pre-identified 210 craters and classified them into different levels. It should be noted that those craters, classified by the two operators as having inconsistent FTPP levels are excluded from this study. Finally, 70 craters located in a relatively narrow range of latitudes (from latitudes 50° to 65°) were selected for the sake of similar sun illumination conditions. Fig. 5 shows the crater distributions with respect to different FTPP levels. From this histogram, it can be seen that most of the craters suffer from serious FTPP problems as indicated in the level 8 and 9 columns. Level 8 contains 33 craters as the biggest group.

To further study the FTPP level distribution pattern as regards the crater shapes, two more charts were generated as shown in Fig. 6. Fig. 6(a) shows the distribution of FTPP levels with respect to crater shapes for all the craters. It can be seen that FTPP is lighter, in general, for craters with smaller depth–diameter ratio values. To analyse the distribution pattern more generally, the average value of the shape ratio *I* are derived for each FTPP level and are plotted and shown in Fig. 6(b). The distribution trend shown in Fig. 6(b) indicates that FTPP levels increase in line with the depth–diameter ratio *I*. This suggests that craters with greater depth–diameter ratio have heaver FTPP problems. The FTPP level distribution trend regarding the average depth–diameter ratio can be modelled by a second-order polynomial as illustrated in Fig. 6(b).

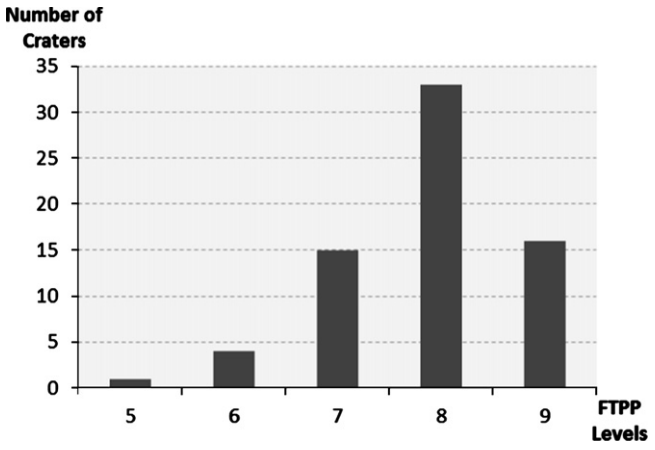

Fig. 5. Histograms of craters suffering from FTPP with respect to different FTPP levels.

4. Remediation of FTPP on Chang'E-1 imagery

This study presents a wavelet-transform based approach for FTPP remediation on Chang'E-1 imagery. The approach employs a digital elevation model (DEM) of the crater area. A SRM with illumination from north-west is derived from DEM. The SRM is then fused to the original crater image by using a shift invariant discrete wavelet transform (SIDWT) method, and the FTPP problem is then alleviated in the resulting image.

4.1. Crater DEM and SRM generation

A high precision crater DEM with a reasonable resolution is important for this method since it is the main contributor to correct the FTTP problem. If the precision of the DEM is low, distortions on the original image will be created during the image fusion. If the resolution of the DEM is distant from the image resolution, the performance of the FTPP correction will then be poor. In this study, the DEMs of craters are generated by using the Chang'E-1 stereo imagery and Chang'E-1 laser altimeter through an integrated photogrammetric method (Wu et al., 2011). The resolution of the DEM is 360 m, which is three times of the resolution of the Chang'E-1 imagery (120 m/pixel) and is good for FTPP correction. Fig. 7 shows the 3D views of the DEM of the crater (named as crater 1) shown in Fig. 1(a). This crater is located in (51.20°N, 43.60°E) with a diameter of 33 km and depth of 3 km.

Based on the DEM, SRMs can be generated with different illumination azimuth angles. Fig. 8 shows the SRMs of crater 1, in which Fig. 8(a) and (b) show the SRMs with an illumination azimuth angle of 315° and 45°, respectively, and Fig. 8(c) and (d) show the SRMs with an illumination azimuth angle of 225° and 135°, respectively. The optimal sun elevation angle in generating these SRMs should be the same with that of the crater in the original image. The sun elevation angles for each row in the Chang'E-1 image are recorded in the meta data of the image, from which the sun elevation angles for specific craters can be derived. The derived sun elevation angle for this crater is 35° and it was used in the generation of all these SRMs. From Fig. 8 it can be seen that, the upper two SRMs have illumination directions from north which agrees with the light-from-front prior assumption and makes them look like craters, while the lower two have illumination directions from south which violates the light-from-front assumption and makes craters look like hillocks.

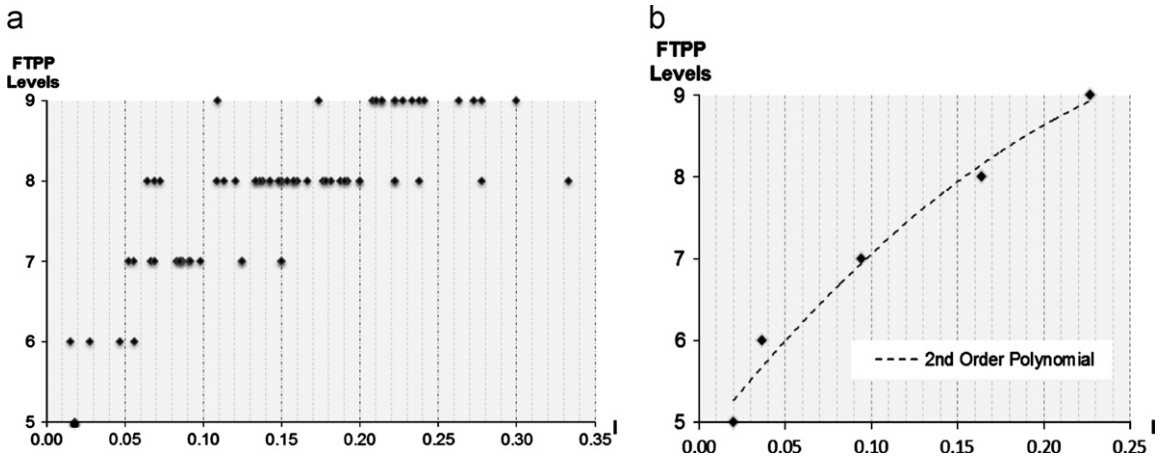

Fig. 6. Distribution of FTPP levels with respect to crater shapes: (a) all craters, and (b) average *I* in each FTPP level.

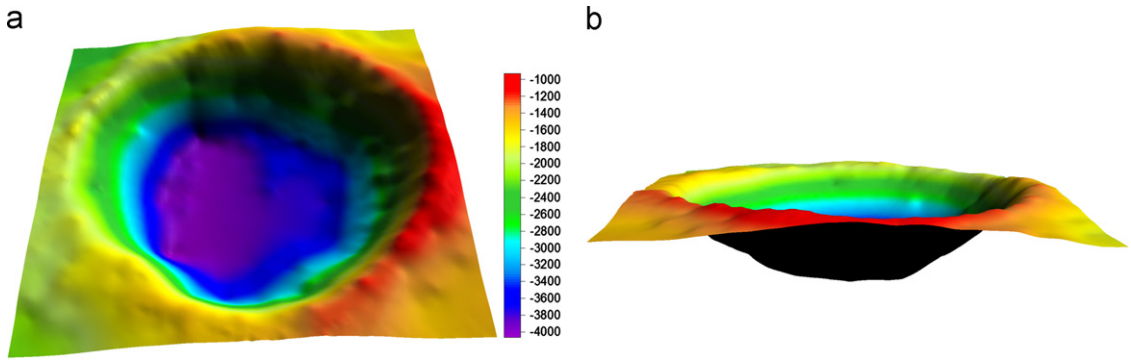

Fig. 7. 3D views of the DEM of crater 1: (a) overhead view, and (b) horizontal view.

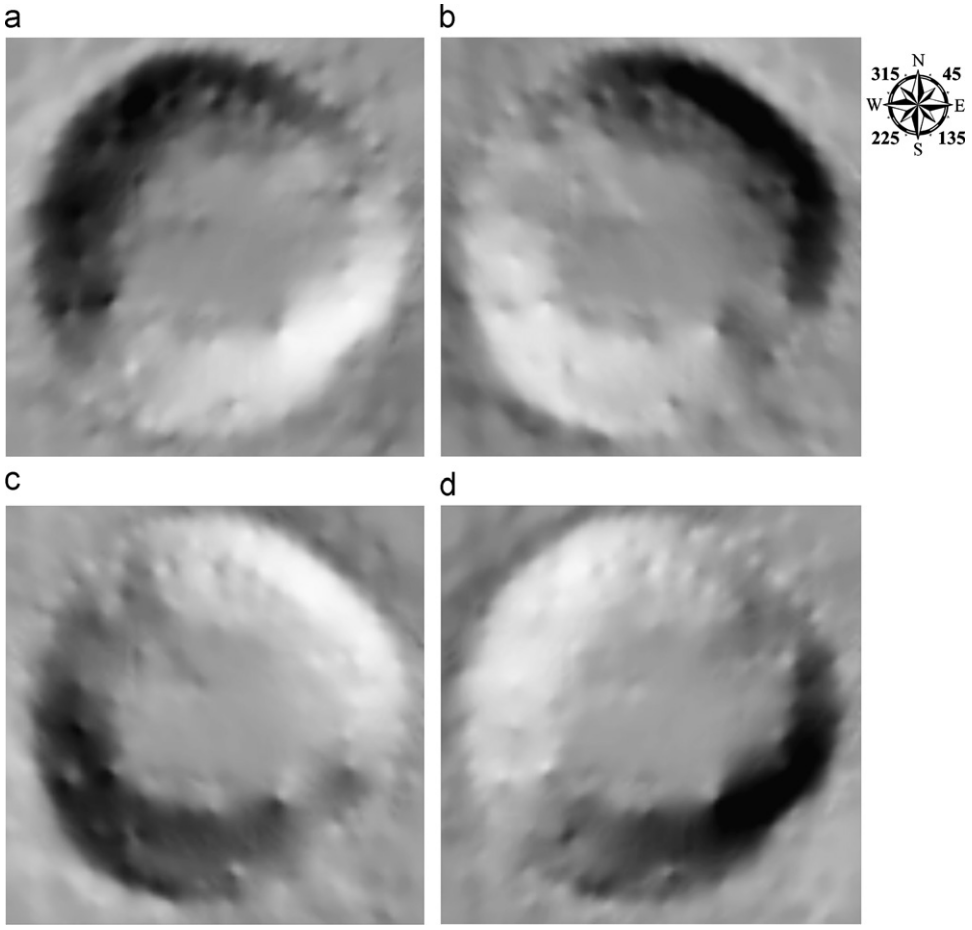

Fig. 8. SRMs of crater 1 generated based on the DEM with illumination azimuth angle of: (a) 315°, (b) 45°, (c) 225°, and (d) 135°.

4.2. Image fusion based on the shift invariant discrete wavelet transform (SIDWT)

Image fusion is a technique of combining relevant information from two or more images into a single image (Graps, 1995), which might be a promising technique to remedy FTPP problems. There are various image fusion techniques presented in the past, such as the intensity-hue-saturation (HIS), principal component analysis (PCA), and wavelet-transform based methods. Wavelets are mathematical functions that cut up data into different frequency components, which can be considered as complements to classical Fourier decomposition method. Wavelet transform allow complex information such as images to be decomposed into elementary forms at different scales and subsequently reconstructed with high precision. In general, wavelet-transform based methods perform better than standard methods such as the HIS and PCA, particularly in terms of minimizing colour distortion (Graps, 1995; Amolins et al., 2007). The discrete wavelet transform (DWT) is a representative wavelet-transform based method and has been widely used in image fusion (Mallat, 1989; Rockinger, 1997).

The DWT method decomposes an image into its multi-scale edge representation, which is based on the fact that the human visual system is primarily sensitive to local contrast changes (i.e., edges). The DWT method includes the following three steps (Rockinger, 1997): (1) The input images are decomposed by DWT to a multi-scale edge representation. (2) A composite multi-scale edge representation is then built by selecting the most prominent wavelet coefficients in the input imagery.

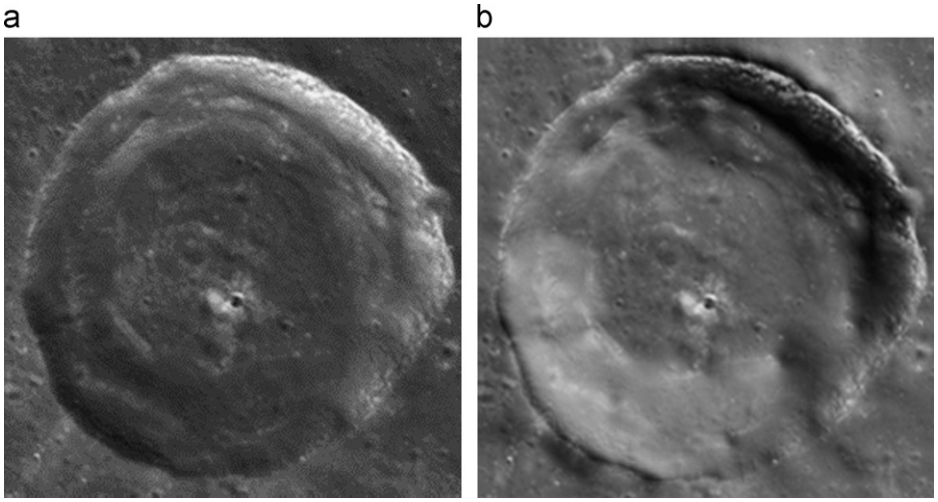

Fig. 9. Fusion results for crater 1 using the wavelet-transform based approach: (a) the original image with FTPP, and (b) the fused image free of FTPP.

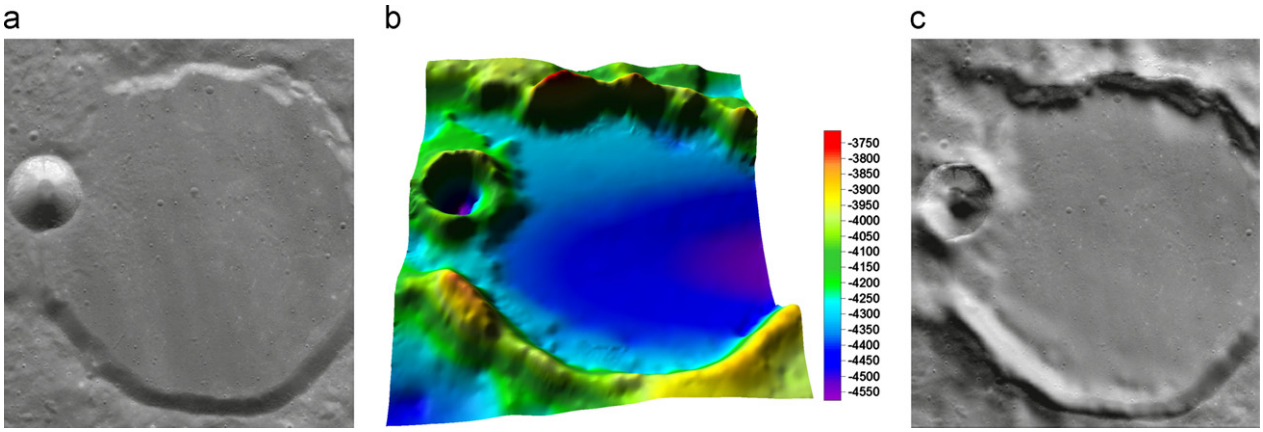

Fig. 10. Experiment for crater 2: (a) the original image of crater 2 suffering from FTPP, (b) the 3D view of the DEM of crater 2, and (c) the resulting image free of FTPP.

The selection is based on a simple maximizing of the coefficients or a sophisticated area-based energy computation. (3) The fused image is computed by an application of the inverse DWT combine the wavelet representation to yield fusion image. Shift invariant DWT (SIDWT) method (Rockinger, 1997; Sari-Sarraf and Brzakovic, 1997) is a shift invariant extension of the standard DWT, which allows generating stable and consistent fusion results. More details about the DWT and SIDWT methods can be found in Rockinger (1997) and Sari-Sarraf and Brzakovic (1997).

This study employs the SIDWT for image fusion. Fig. 9 shows an example of the fusion results for crater 1. In Fig. 9, the original image is fused with the SRM with an illumination azimuth angle of 45° as shown in Fig. 8(b), and the results are shown in Fig. 9(b). From the results, it is clear that the FTPP problem has been effectively alleviated.

4.3. Further experiments and evaluation

Two additional craters (craters 2 and 3) with different characteristics from crater 1 were tested using the developed method. Crater 2 is located in (58.56°N, 86.96°E) with a diameter of 52 km and depth of 0.8 km. Crater 2 is much flatter than crater 1. Fig. 10(a) shows the original image of crater 2 and Fig. 10(b) shows its DEM.

By using the wavelet-transform based approach, an FTPP-free image for crater 2 is generated shown in Fig. 10(c). It is seen that the FTPP problem in the resulting image has been effectively alleviated compared with that in the original image.

Crater 3 is located in (55.33°N, 118.33°W) with a diameter of 32 km and depth of 3.5 km. This crater has a similar size and shape with crater 1, but has more illumination exposure than crater 1. Fig. 11(a) shows the original image of crater 3 and Fig. 11(b) shows its DEM.

By using the wavelet-transform based approach, an FTPP-free image for crater 3 is generated as shown in Fig. 11(c), indicating that the FTPP problem has been effectively alleviated.

Comparing the FTPP remediated images with the original images for craters 1, 2, and 3, it can be noticed that the remediation process may cause slight deviations from the exact perception of the crater morphology. However, the described remediation method is still valuable since it corrects FTPP problems to avoid obvious wrong perceptions.

To evaluate the performances of the method presented in this paper, a questionnaire survey has been carried out with 31 people who have various backgrounds and no previous knowledge of FTPP. The questionnaire contains 6 questions. In response, the interviewees, have to identify the FTPP levels of each of the three craters tested in this study under two different conditions. They are the original image and the image after FTPP remediation using the wavelet-transform based approach. The FTPP levels are classified following the scheme given above: level 5–9 with 5 represent light FTPP and 9 represents heavy FTPP, while the other four levels are added to evaluate the depth perception strength (level 1–4 with 1 representing strong depth perception and 4 representing relatively weak depth

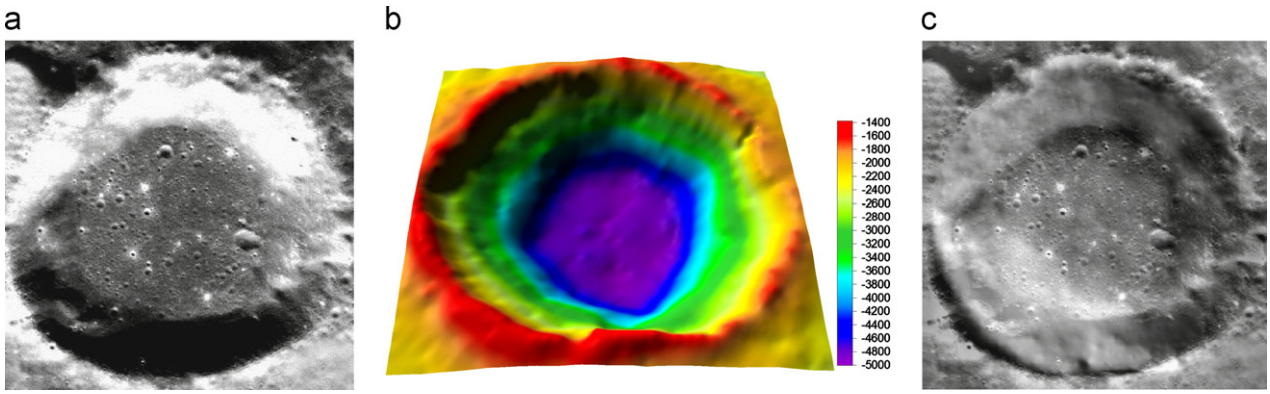

Fig. 11. Experiment for crater 3: (a) the original image of crater 3 suffering from FTPP, (b) the 3D view of the DEM of crater 3, and (c) the resulting image free of FTPP.

Table 2
Summary of the survey outputs.

	Original image	Image after FTPP remediation
Crater 1		
Average	6.18	3.34
Stdev	1.42	1.72
Crater 2		
Average	5.96	3.82
Stdev	0.56	0.89
Crater 3		
Average	7.34	2.8
Stdev	2.01	1.73

perception). The outputs of the survey are summarized in Table 2.

From Table 2, it is clearly seen that the three experimental craters all contain FTPP problems since their average FTPP levels are all larger than 5. After the remediation using the wavelet-transform based approach, the FTPP levels dropped to 3.34, 3.82 and 2.8. This indicates that the approach works effectively. Table 2 also lists the standard deviations for each case. Here it can be seen that the responses from the interviewees are quite consistent for crater 2 and relatively dispersed for carters 1 and 3.

5. Conclusions and discussion

This paper presents a systematic investigation of the FTPP problem observed in the Chang'E-1 lunar imagery and also presents an effective method for FTPP remediation. The analysis and experimental results lead to the following conclusions:

(1) The FTPP problem associated with craters revealed by lunar imagery is positively correlated with the latitudes of craters in the northern hemisphere of the Moon, and for craters within similar latitude ranges, the FTPP level is positively correlated with the depth–diameter ratio of the crater;
(2) The wavelet-transform based approach is able to correct FTPP problems. Experiments and survey revealed that the FTPP problem can be effectively alleviated after applying the proposed approach.

It should be noted that, this investigation is based on the selected study areas covering the latitudes from -70° to 70° of the lunar surface. The extreme cases in the north pole region are not included in this investigation. A systematic investigation about the FTPP problems in the north pole region and generation of crater DEMs with favorable resolution from other data source (e.g., the LRO NAC images or Laser Altimeter data) for FTPP remediation in the north pole region will be our future efforts.

Acknowledgment

The authors would like to thank the National Astronomical Observatories of the Chinese Academy of Sciences for providing the Chang'E-1 data sets. The work described in this paper was supported in part by a grant from the Research Grants Council of Hong Kong under Project PolyU 5312/10E and in part by the Hong Kong Polytechnic University under Grant A/C 1-BB83. The work was also partially supported by a State 973 project of China (♯2012CB719901).

References

Amolins, K., Zhang, Y., Dare, P., 2007. Wavelet based image fusion techniques—an introduction, review and comparison. ISPRS Journal of Photogrammetry and Remote Sensing 62 (4), 249–263.
CAS (Chinese Academy of Sciences), 2008. Working References for the Lunar Explorer Project Scientific Application Users. Chinese Academy of Sciences, Lunar Exploration Project, General Design Section, pp. 140.
Colby, J.D., 1991. Topographic normalization in rugged terrain. Photogrammetric Engineering and Remote Sensing 57 (5), 531–537.
Graps, A., 1995. An introduction to wavelets. IEEE Computational Science and Engineering 2 (2), 50–61.
Ivanov, B.A., 2001. Mars/Moon cratering rate ratio estimates. Chronology and Evolution of Mars 96, 87–104.
Kumar, A.S.K., Chowdhury, A.R., 2005. Terrain mapping camera for Chandrayaan-1. Journal of Earth System Science 114 (6), 717–720.
Liu, B., Todd, J.T., 2004. Perceptual biases in the interpretation of 3D shape from shading. Visual Research 44 (18), 2135–2145.
Mallat, S.G., 1989. A theory for multiresolution signal decomposition: the wavelet representation. IEEE Transactions on Pattern Analysis and Machine Intelligence 11 (7), 674–693.
Morgenstern, Y., Murray, R.F., Harris, L.R., 2011. The human visual system's assumption that light comes from above is weak. Proceedings of the National Academy of Sciences of the United States of America (PNAS) 108, 12551–12553.
Moutsoulas, M., Preka, P., 1981. Morphological characteristics of lunar craters with moderate depth/diameter ratio. Earth, Moon, and Planets 25 (1), 51–66.
Ouyang, Z.Y., Li, C., Zou, Y., Zhang, H., Lv, C., Liu, J., Liu, J., Zuo, W., Su, Y., Wen, W., 2010. Preliminary scientific results of Chang'E-1 lunar orbiter. Science China 53 (11), 1565–1581.
Patterson, T., Kelso, N.V., 2004. Hal Shelton revisted: designing and producing natual-color maps with satellite land cover data. Cartographic Perspectives 47, 28–55.
Ramachandran, V.S., 1988a. Perception of shape from shading. Nature 331 (6152), 133–166.
Ramachandran, V.S., 1988b. Perceiving shape from shading. Scientific American 259 (2), 76–83.
Rieser, J.J., Pick, H.L., Ashmead, D.H., Garing, A.E., 1995. Calibration of human locomotion and models of perceptual motor organization. Journal of Experimental Psychology: Human Perception and Performance 21 (3), 480–497.
Robinson, M.S., Brylow, S.M., Tschimmel, M., Humm, D., Lawrence, S.J., Thomas, P.C., Denevi, B.W., Bowman-Cisneros, E., Zerr, J., Ravine, M.A., Caplinger, M.A., Ghaemi, F.T., Schaffner, J.A., Malin, M.C., Mahanti, P., Bartels, A., Anderson, J.,

Tran, Y., Eliason, E.M., McEwen, A.S., Turtle, E., Jolliff, B.L., Hiesinger, H., 2010. Lunar Reconnaissance Orbiter Camera (LROC) instrument overview. Space Science Reviews 150 (1–4), 81–124.

Rockinger, O., 1997. Image sequence fusion using a shift-invariant wavelet transform. Proceedings of the 1997 International Conference on Image Processing, pp. 288–291.

Rudnicki, W., 2000. The new approach to the relief shading applied in the satellite image maps. Proceedings of the Second Symposium of the Commission on Mountain Cartography, pp. 105–106.

Saraf, A.K., Das, J., Agarwal, B., Sundaram, R.M., 1996. False topography perception phenomena and its correction. International Journal of Remote Sensing 17 (18), 3725–3733.

Saraf, A.K., Ghosh, P., Sarma, B., Choudhury, S., 2005. Development of a new image correction technique to remove false topographic perception phenomena. International Journal of Remote Sensing 26 (8), 1523–1529.

Saraf, A.K., Sinha, S.T., Ghosh, P., Choudhury, S., 2007. A new technique to remove false topographic perception phenomenon and its impacts in image interpretation. International Journal of Remote Sensing 28 (5), 811–821.

Saraf, A.K., Zia, M., Das, J., Sharma, K., Rawat, V., 2011. False topographic perception phenomena observed with the satellite images of Moon's surface. International Journal of Remote Sensing 32 (24), 9869–9877.

Sari-Sarraf, H., Brzakovic, D., 1997. A shift-invariant discrete wavelet transform. IEEE Transactions on Signal Processing 45 (10), 2621–2626.

Stepinski, T.F., 2010. Geographical distribution of crater depths on Mars. Proceeding of the 41st Lunar and Planetary Science Conference, The Woodlands, Texas, March 1–5, 2010.

Toutin, T., 1998. Depth Perception with Remote Sensing Data. In Future Trends in Remote Sensing (edited by P. Gudmandsen: A.A. Balkema), pp. 401–409.

Wu, B., Guo, J., Zhang, Y., King, B., Li, Z., Chen, Y., 2011. Integration of Chang'E-1 imagery and laser altimeter data for precision lunar topographic modeling. IEEE Transactions on Geoscience and Remote Sensing 49 (12), 4889–4903.